

Out-of-plane permittivity of confined water

H. Jalali,^{1,2} H. Ghorbanfekr,³ Ilyar Hamid,³ M. Neek-Amal^{2,3,*}, R. Rashidi,² and F. M. Peeters³

¹*Department of Physics, University of Zanjan, 45195-313, Zanjan, Iran*

²*Department of Physics, Shahid Rajaee Teacher Training University, 16875-163, Lavizan, Tehran, Iran*

³*Department of Physics, Universiteit Antwerpen, Groenenborgerlaan 171, B-2020 Antwerpen, Belgium*



(Received 8 September 2019; revised 3 March 2020; accepted 1 July 2020; published 11 August 2020)

The dielectric properties of confined water is of fundamental interest and is still controversial. For water confined in channels with height smaller than $h = 8 \text{ \AA}$, we found a commensurability effect and an extraordinary decrease in the out-of-plane dielectric constant down to the limit of the dielectric constant of optical water. Spatial resolved polarization density data obtained from molecular dynamics simulations are found to be antisymmetric across the channel and are used as input in a mean-field model for the dielectric constant as a function of the height of the channel for $h > 15 \text{ \AA}$. Our results are in excellent agreement with a recent experiment [L. Fumagalli *et al.*, *Science* **360**, 1339 (2018)].

DOI: [10.1103/PhysRevE.102.022803](https://doi.org/10.1103/PhysRevE.102.022803)

I. INTRODUCTION

Water adsorbed in nanopores exhibits anomalous properties including fast flow in nanochannels, distinct melting points, structural phase transitions, layering, and ultralow dielectric constant [1–5]. In confining geometries, the polarization of water is different from bulk water which affects the water-mediated intermolecular forces and consequently changes hydration and solvation, as well as molecular transport properties. In the past few decades, the main theoretical method for studying dynamical and structural properties of confined water was based on molecular dynamics simulations (MDS). A large variety of classical force fields has been applied to describe water-water and water-interface interactions under both normal and critical conditions [6–17]. For instance, the variation of the dielectric constant with temperature and pressure for ices Ih, III, V, VI, and VII was studied by Aragonés *et al.* [17]. In addition to MDS, mean-field theory (such as Kirkwood’s theory) was also used and yields valuable insights into the H-bonding effects on the dielectric constant of water [18,19].

By using electrostatic force detection with an atomic force microscope (AFM), unexpected variation in the dielectric constant of confined water between graphene (GE) and hexagonal boron nitride (h-BN) was observed recently as a function of the thickness of the channels [20]. A small out-of-plane dielectric constant of about $\simeq 2.1$ for nanoconfined water in channels with heights $h \sim 10 \text{ \AA}$ was reported [20], but the underlying physics is not understood. Beyond $\sim 15 \text{ \AA}$ a nonlinear increase in the dielectric constant was found and a phenomenological capacitance model was used to interpolate the dielectric constant of nanoconfined water and bulk water. Here we show that a fundamental ingredient was missing in the phenomenological model: the wall-induced dipole in the water surface layers which turns out to have a considerable

effect on the dielectric properties of confined water. When including this effect, we find an almost perfect agreement with experiment.

In this paper, polarization density obtained from rigorous MDS is used as input for a mean-field model providing the dielectric properties of confined water without fitting parameter. In particular, we found the perpendicular component of the dielectric constant (ϵ_{\perp}) of confined water for channels with height ranging from angstrom up to micrometer. Moreover, for channels with height $h \approx 7.5 \pm 0.5 \text{ \AA}$, we predict an extraordinary decrease in ϵ_{\perp} which is due to an increase in the number of H bonds in the system and a phase transition to dense amorphous ice. We further link the capacitance model (C model) [20,21] to the microscopic details of confined water and determine the wall-induced dipoles and corresponding dielectric constant. For the ice phase of water, the number of hydrogen bonds is slightly larger than for liquid. The pronounced peak in the inset of Fig. 1(b) is due to the formation of an amorphous phase of ice in the channels when $h \approx 7.5 \pm 0.5 \text{ \AA}$.

II. MODEL AND METHOD

We performed MDS of nanoconfined water between two parallel graphene and hexagonal boron nitride sheets using the LAMMPS package [22]. We used the SPC/E [23] potential. Simulations were carried out in the *NVT* ensemble at $T = 300 \text{ K}$. The area of the computational unit cell was taken as $A = 42^2 \text{ \AA}^2$ (for more details, see Supplemental Material and Fig. S1 therein [24]). The cell length along the z axis was changed by subangstrom steps of about 0.2 \AA for $h < 10$ and 1 \AA beyond $h = 10 \text{ \AA}$. Note that in all plots “ h ” is the distance between the center of two C atoms of top and bottom graphene layers; however, for the calculation of density, out-of-plane permittivity, etc., we used the effective height (as shown in the left-hand side of Supplemental Material Fig. S1 [24]), i.e., $h^{\text{eff}} = h - \sigma$ where σ is the length parameter

*mehdi.neekamal@gmail.com

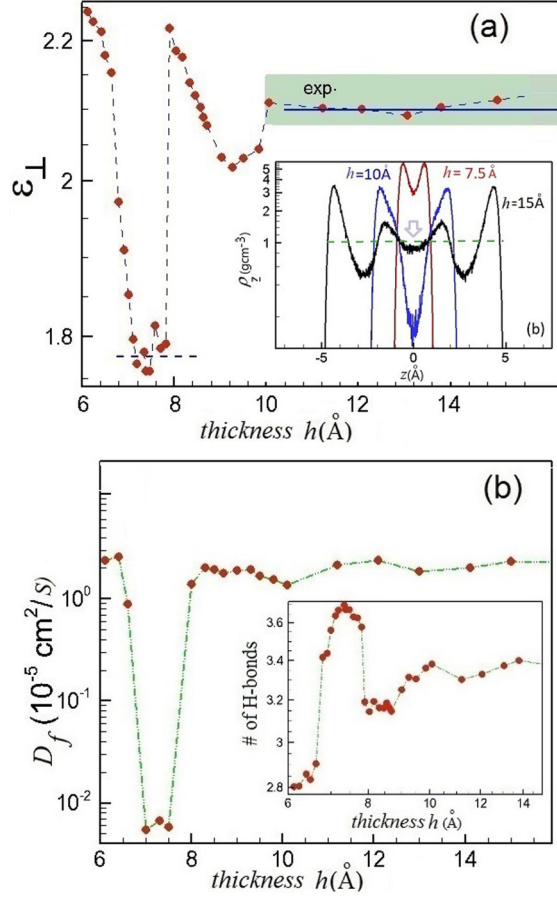


FIG. 1. The variation of ϵ_{\perp} with respect to the height of the channel for nanoconfined water between two graphene sheets which are separated by distance h . The shaded area denotes the error bar of the experimental data of Ref. [20]. The bottom dashed line refers to $\epsilon_{\perp} = n^2$, which is the dielectric constant of water at optical frequencies where $n = 1.33$ is the refractive index. The inset shows the formation of surface water layers close to the graphene sheets for $h = 7.5$ Å, $h = 10$ Å, and $h = 15$ Å. When $h = 15$ Å other water molecules are intercalated between those water surface layers resulting in the growth of the middle bulklike region. (b) The in-plane diffusion coefficient of confined water as a function of the size of the channel. The inset shows the variation of the corresponding number of H bonds.

in the Lennard-Jone potential. In this way we included the excluded volume because of the finite size of both carbon atoms (confining walls) and water molecules. Taking the carbon-carbon distance (h) for the volume estimation causes an underestimation of the density of intercalated water.

III. DENSITY PROFILE

In the inset of Fig. 1(a) we depict the variation of the mass density (ρ_z) across the channel for three different h , i.e., $h = 7.5$, 10, and 15 Å. In the channel with height $h = 7.5$ Å two distinguishable large peaks appear [this is related to the nucleation of the surface water layers (SLs) [15,16,25]]. Note that the density at the peaks is $\rho_z \simeq 5.5$ g cm $^{-3}$, which is substantially larger than the bulk density $\rho_B = 1$ g cm $^{-3}$ and the density between two peaks is $\rho_z \simeq 3\rho_B$. By increasing

the height of the channel up to $h = 10$ Å, two layers (having smaller peaks and an almost empty middle part with $\rho_z \ll \rho_B$) are formed: i.e., bilayer ice [7,26]. By increasing the channel size further, the height of the peaks remain constant (see density for $h = 15$ Å). For $h = 10$ Å the two surface water layers are well separated and consequently we can define the thickness of the surface water layer as $D \approx (10.0 - \sigma)/2 \simeq 3.4$ Å where $\frac{\sigma}{2}$ is the thickness of the exclusion area at the graphene-water interface [4,27]. This number is close to the one reported by Cicero *et al.* [27], i.e., $D \approx 3.0$ Å, and is within the range reported by Zhang [21], i.e., 1.5–4.5 Å. For the larger channels (e.g., $h = 15$ Å) other smaller density peaks appear between the two layers. In fact, for the larger channels, more water molecules intercalate between the SLs and consequently a large flat region between two SLs starts to develop [highlighted by the arrow in the inset of Fig. 1(a)].

IV. DIELECTRIC CONSTANT: ANGSTROM THIN CHANNELS ($h < 15$ Å)

We performed extensive MDS by including microscopic details of nanoconfined water in channels with $h < 15$ Å. In fact, when a water slab is subjected to a weak electric field the local perpendicular component of the dielectric constant at distance z can be calculated by using [15,16]

$$\epsilon_{\perp}^{-1}(z) = 1 - \frac{\delta_{\perp}^2(z)}{\epsilon_0 k_B T + \delta_{\perp}^2/V}, \quad (1)$$

where ϵ_0 is the vacuum permittivity, $V = Ah$ is the volume of the simulation box, $\delta_{\perp}^2(z) = \langle m_{\perp}(z)M_{\perp} \rangle - \langle m_{\perp}(z) \rangle \langle M_{\perp} \rangle$ with $m_{\perp}(z)$ the spatial resolved microscopic polarization density, and $M_{\perp} = A \int m_{\perp}(z) dz$ the total dipole moment of the system. In Eq. (1) $\Sigma_{\perp}^2 = A \int \delta_{\perp}^2(z) dz$ and the perpendicular polarization density profile $m_{\perp}(z)$ is calculated using the integral of the local electron distribution $\varrho(z)$, i.e., $m_{\perp}(z) = - \int_{-h/2}^z \varrho(z') dz'$. Note that we found that $\Sigma_{\perp}^2 \simeq \delta^2 V$, which can be due to the in-plane homogeneous mass density distribution within each SL. This is an important finding which substantially decreases the simulation time.

The averaging and correlations were taken over more than 10 ns after $\epsilon_{\perp}(z)$ was converged. In Fig. S2 of the Supplemental Material [24] we show the results (time series) obtained from MDS using Eq. (1) for a channel with height $h = 10$ Å. The result converges to $\epsilon_{\text{SL}} = 2.102(2)$. Consequently, the effective dielectric constant ($\bar{\epsilon}_{\perp}$) can be obtained using

$$\frac{1}{\bar{\epsilon}_{\perp}} = \frac{1}{h^{\text{eff}}} \int_{-h^{\text{eff}}/2}^{h^{\text{eff}}/2} \frac{dz}{\epsilon_{\perp}(z)}, \quad (2)$$

where $h^{\text{eff}} = h - \sigma$ is the effective height of the channel. In Fig. 1(a), we depict the variation of ϵ_{\perp} with channel height for $h < 15$ Å. It is seen that for channels with height 6.7 Å $< h < 8$ Å there is a deep local minimum. Beyond $h = 8$ Å, the dielectric constant, as shown in Fig. 1, approaches $\epsilon_{\text{SL}} = 2.1$. Our results are in good agreement with experiments [20], which were done for $h > 8$ Å [shaded area in Fig. 1(a)].

To obtain further insights, we evaluated the in-plane component of the diffusion coefficient [$D_f = (D_{xx} + D_{yy})/2$] of systems with different channel heights using the mean-square displacement method [28]. The results are shown in Fig. 1(b).

A significant decrease in the diffusion coefficient is found which is an independent check for the presence of a phase transition from liquid water to amorphous ice. Such a phase transition is known and was already reported by Zangi *et al.* [29]. It is related to commensurability effects in confined water [6]. Moreover, we calculated the number of hydrogen bonds (H bonds) for different channel heights [see inset of Fig. 1(b)]. There is a significant peak within the range $h = 6.7\text{--}8 \text{ \AA}$ which is a consequence of the aforementioned structural transition of liquid water to amorphous ice. We found a direct correlation, i.e., $r = +0.91$ (anticorrelation, $r = -0.89$) between ϵ_{\perp} and D_f (number of hydrogen bonds). Note that both ϵ_{\perp} and D_f exhibit an oscillatory behavior which is a consequence of the commensurability effect beyond 6 \AA , i.e., optimal layering of water.

V. DIELECTRIC CONSTANT: FROM NANOMETER TO BULK THICK CHANNELS

Here we explain the C model that was used in Ref. [20] to explain the experimental data for ϵ_{\perp} for channels with $h \geq 20 \text{ \AA}$. They modeled the system as consisting of three capacitors in series and the total capacitance is given by [20] $C_T^{-1} = C_L^{-1} + C_m^{-1} + C_R^{-1}$. It was assumed that the capacitance of the surface water layer (called “dead layer” in Ref. [20]) was taken as $C_L = C_R$, which indicates that the two near-surface layers (SLs) have the same capacitance and consequently equal dielectric constant [20].

Thus, in order to interpolate the perpendicular component of the dielectric constant from the angstrom regime to bulk water, we introduce an imposed C model [20,21]. Confined water is divided into *three parts*, i.e., two SLs (formed near the confining walls) with dielectric constant $\bar{\epsilon}_L$ and $\bar{\epsilon}_R$, and the middle region having dielectric constant $\bar{\epsilon}_m$. We use symbol “L” (“R”) for the left (right) SL and assume that the external electric field is along the $+z$ axis, i.e., from the bottom to the top. It is known that [21]

$$\bar{\epsilon}_{\perp}^{-1} = \frac{D}{h} \epsilon_{\text{SL}}^{-1} + \frac{h - 2D}{h} \bar{\epsilon}_m^{-1}, \quad (3)$$

where $\epsilon_{\text{SL}}^{-1} = \frac{1}{2}(\bar{\epsilon}_L^{-1} + \bar{\epsilon}_R^{-1})$. In order to calculate $\bar{\epsilon}_{\perp}$ for a given channel, we found the local polarization density (LPD). In the absence of an external electric field, the z component of the LPD was calculated $p_{\perp}(z, E_0 = 0) = \delta\mathcal{P}/\delta V$, where $\delta\mathcal{P}$ is the net dipole moment of volume δV . By dividing h into N small slabs with thickness δz ($h = N\delta z$), we find the LPD [$p_{\perp}(z, 0)$] as shown in Fig. 2 (dots) for $h = 7.5 \text{ \AA}$ (the surface area of the computational unit cell along the confining walls was taken $A = 42^2 \text{ \AA}^2$). There are peaks at $z_0 \approx \pm 0.6 \text{ \AA}$ in the $p_{\perp}(z, 0)$ profile which are related to the net dipole of each SL and correspond with the maximum in the density profile [see inset of Fig. 1(a)]. For channel $h = 10 \text{ \AA}$ the result is shown in the inset where a small flat region appears between the two peaks [$p_{\perp}(z, 0)$ of the two SLs], which is highlighted by the arrow in the inset. The polarization of SLs (when $E_0 = 0$) with opposite directions are due to the exerted van der Waals torque on the water molecules close to the confining walls [7]. The flat region with small LPD between the two peaks is due to the random orientation of water molecules in the semibulk.

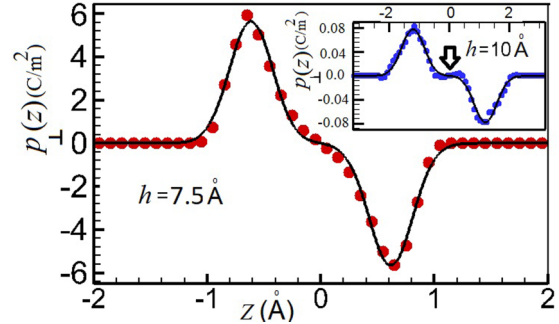


FIG. 2. The variation of local polarization density across a channel with $h = 7.5$ and 10 \AA (see inset) filled by water. The orientation of the water molecules close to the graphene sheets is shown in the inset.

VI. THE POLARIZATION DENSITY AND DIELECTRIC CONSTANT OF THE “SURFACE WATER LAYERS”

In order to find the out-of-plane dielectric constant of both SLs, we focus on the channel with height $h = 10 \text{ \AA}$ where the two SLs are most clearly defined. We find the best fits (solid line in the inset of Fig. 2) of the $p_{\perp}(z, 0)$ data with the following equations:

$$p_L(z < 0, E_0 = 0) \simeq A_1 e^{-(z+z_0)^2/2\sigma_0^2}, \quad (4a)$$

$$p_R(z > 0, E_0 = 0) \simeq -A_2 e^{-(z-z_0)^2/2\sigma_0^2}, \quad (4b)$$

where p_L (p_R) are the LPD of the left (right) SL with amplitude A_1 (A_2). In fact, these two variables are LPD of SLs in the absence of external electric field. Obviously, because of the geometrical symmetry $p_L(z, 0) = -p_R(-z, 0)$ (see solid curves in Fig. 2). Using a mean-field approach in the presence of external electric field E_0 , the local dielectric constant for each SL is given by [16,19,30,31]

$$\bar{\epsilon}_{L,R}^{-1}(z, E_0) = 1 - \Delta p_{L,R}(z, E_0)/\epsilon_0 E_0, \quad (5)$$

where the induced macroscopic polarization density due to the applied field is $\Delta p_{L,R} = p_{L,R}(z, E_0) - p_{L,R}(z, 0)$. We found that $\Delta p_{L,R}(z, E_0)$ are two symmetric functions of z and $p_{L,R}(z, E_0) > p_{L,R}(z, 0)$.

The MDS results for the local polarization density and $\Delta p_{\perp}(z, E_0)$ are shown in Fig. 3 for $h = 100 \text{ \AA}$ (and in the inset for $h = 10 \text{ \AA}$) when $E_0 = 0$ and $E_0 = 0.1 \text{ V \AA}^{-1}$. The symmetrical properties are independent of the thickness of the channel. The corresponding $\Delta p_{\perp}(z, E_0)$ are shown by black curves. Though the LPDs are antisymmetric [see Eqs. (4)], $\Delta p_{\perp}(z, E_0)$ are symmetric. This will result in $\epsilon_R = \epsilon_L$. On the other hand, in order to find $\langle \Delta p_{\perp}(E_0, h) \rangle$, we performed five additional MDS for channels with height $h = 13, 24, 44, \text{ and } 83 \text{ \AA}$ and bulk water. By applying a weak electric field of $E_0 = 0.01 \text{ V \AA}^{-1}$, we calculated $\Delta p_{\perp}(E_0, h)$ and found that it could be fitted to $p_B e^{-D/h}$ with $p_B = 8.75 \times 10^{-4} \text{ C m}^{-2}$ and $D = 3.4 \text{ \AA}$ (see Supplemental Material Fig. S3 [24]). Notice that in general p_B is a function of E_0 . The exponential increase of the macroscopic polarization of the middle region is an indication of the importance of correlations between the SLs and water molecules outside of the SLs. In the Supplemental Material Fig. S4 [24] we depict the variation of ϵ_m with channels height when $E_0 = 0.01 \text{ V \AA}^{-1}$

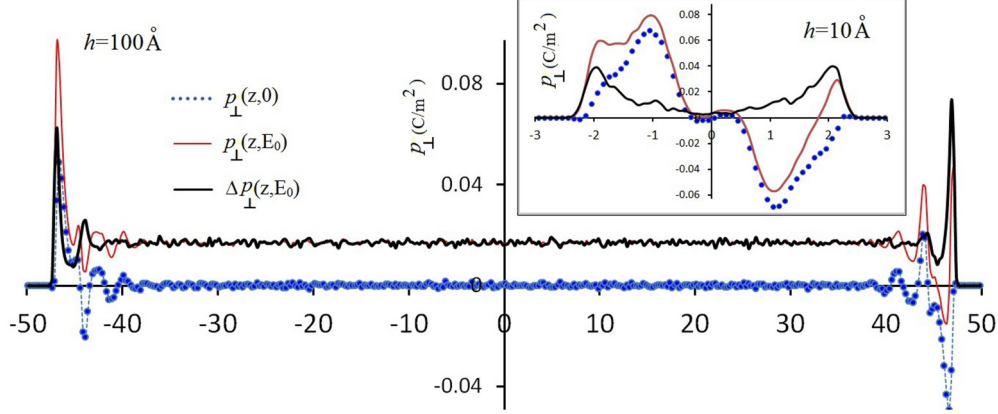


FIG. 3. The local polarization density across the channel [$p_{\perp}(z, E_0)$] for an applied electric field of $E_0 = 0$ and $E_0 = 0.1 \text{ V \AA}^{-1}$ for channel height $h = 100 \text{ \AA}$ and $h = 10 \text{ \AA}$ (inset) in the absence (presence) of electric field is shown by blue dots (red curve). The differences between these two data are shown by the black curve.

which confirms the large height limit of $\epsilon_m \simeq 80$. For instance, in Fig. S3 of the Supplemental Material [24], we show MDS results of the LPD and Δp_{\perp} for $h = 10 \text{ \AA}$ and $h = 100 \text{ \AA}$ when $E = 0.0$ and $E_0 = 0.1 \text{ V \AA}^{-1}$. The blue dotted curve is the results for $p_{\perp}(z, 0)$ and the red curve is the LPD data in the presence of $E_0 = 0.1 \text{ V \AA}^{-1}$. Interestingly the results for Δp_{\perp} are symmetric confirming that the latter symmetrical effect is independent of the thickness of the channel. The absence of perfect symmetry in the polarization for channels with height $h = 100 \text{ \AA}$ is due to the smaller statics of MD simulations as compared to the statics for $h = 10 \text{ \AA}$. The large number of water molecules in the system when $h = 100 \text{ \AA}$ makes the simulations time-consuming. Eventually, the corresponding effective dielectric constant of SLs is obtained from

$$\bar{\epsilon}_{L,R}^{-1} = \frac{1}{D} \int_{L,R} \frac{dz}{\epsilon_{L,R}(z, E_0)}. \quad (6)$$

Notice that $\bar{\epsilon}_L = \bar{\epsilon}_R$. The effective dielectric constant of the SL when $h = 10 \text{ \AA}$ and $E_0 = 0.1 \text{ V \AA}^{-1}$ is found to be $\bar{\epsilon}_{L,R} \simeq 1.98$. The latter number is close to our obtained value for $\epsilon_{SL} \simeq 2.1$ using MDS.

VII. THE EFFECT OF DENSITY OF WATER INSIDE THE CHANNELS

In order to determine the number of water molecules inside a channel with height h , we connect the channels to two reservoirs (as we discussed in detail in Refs. [4,32]). The density of water in the reservoirs is kept constant at the bulk density with $P_0 = 1 \text{ atm}$ (e.g., by using two moving walls; see Refs. [4,32]). The density of water molecules inside the channel can be determined by counting the number of water molecules inside the channel divided by the effective volume [4,33]. The ratio between the chemical potential of water outside and inside the channel is proportional to the minus of the ratio between the corresponding pressures [4,34]. We found that the density of water inside channels with $h < 15 \text{ \AA}$ can be slightly larger than the density of bulk, and beyond $h = 15 \text{ \AA}$ the density approaches the bulk density. In order to show the effects of density we plot in Supplemental

Material Fig. S5 [24] the dielectric constant ϵ_{\perp} as a function of density.

VIII. COMPARISON WITH EXPERIMENT

The capacitance of the middle region is determined by performing additional MDS. The polarization density of the middle region is averaged over z and approaches the polarization density of bulk water in the presence of E_0 , i.e., $p_B = \langle \Delta p_{\perp}(E_0, h \rightarrow \infty) \rangle$. For intermediate values of h this polarization density is influenced by the dipoles of the surface water layers and by the spatial density oscillations [see curve for $h = 15 \text{ \AA}$ in Fig. 1(b)]. However, from MDS we found that it can be approximated by $\langle \Delta p_{\perp}(E_0, h) \rangle \approx p_B e^{-D/h}$. Accordingly the dielectric constant of the middle region is given by

$$\frac{1}{\bar{\epsilon}_m(h, E_0)} = 1 - \frac{p_B}{\epsilon_0 E_0} e^{-D/h}. \quad (7)$$

For $h \gg 15 \text{ \AA}$, one naturally expects to recover the dielectric constant of bulk water. The obtained $p_B = 8.75 \times 10^{-4} \text{ C m}^{-2}$ and $D = 3.4 \text{ \AA}$ for $E_0 = 0.01 \text{ V/\AA}$ (see Supplemental Material Fig. S4 [24]) guarantees that $\epsilon_m(h \rightarrow \infty, E_0) \simeq 80 \pm 5$.

Using Eqs. (3) and (7), the effective dielectric constant of a slab of water confined between two graphene sheets can be calculated. The obtained ϵ_{\perp} for $h \geq 15 \text{ \AA}$ are shown by the solid curve in Fig. 4 for $D = 3.4 \text{ \AA}$. The results are compared with the C model of Ref. [20] where the thickness of the surface layer was used as a fitting parameter ($D = 7.4 \text{ \AA}$). Notice that $D = 7.4 \text{ \AA}$ is almost twice the thickness $D = 3.4 \text{ \AA}$ of the surface water layer as determined microscopically. Notice that the present approach does not involve any fitting parameter and gives much better agreement with experiment (red dots). We also compared our results with those of Refs. [30,31], which overestimate ϵ_{\perp} when compared with experiment and our results (see square symbols in Fig. 4).

It is worthwhile to mention that we repeated all the calculations for channels made of h-BN using the water-hBN potential introduced by Wu *et al.* [35], and found similar results for $h < 15 \text{ \AA}$. Therefore, we conclude that confinement

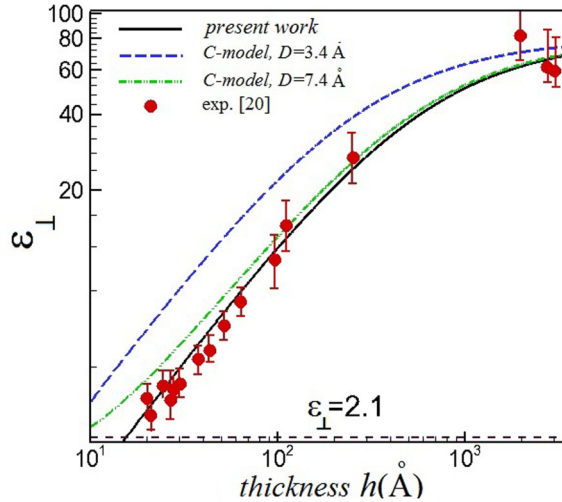


FIG. 4. The dielectric constant of confined water in channels having size $h \geq 15$ Å. The experimental data are shown by orange dots. The dashed lines are the results of the capacitance model used in Ref. [20] with $D = 3.4$ Å (blue) and $D = 7.4$ Å (green). The results of Refs. [30,31] are depicted by square symbols.

is the main origin of the found interesting behavior of ϵ_{\perp} with h . In our previous paper [36], we showed that the electronic contribution to the dielectric constant of confined two-dimensional ice is within the range 1.4–2.0 at 0 K. At room temperature, the electronic dielectric constant of confined water at angstrom scale slits should be smaller, i.e., 1.2. We found that the charge density of water in two-dimensional space is suppressed by the confinement along the z axis. The latter effect makes the electronic contribution smaller (than what is expected from bulk water) and negligible. Nevertheless, what we report in this study is the dipolar contribution which is straightforwardly obtained using Eq. (2).

IX. CONCLUSION

In summary, our imposed C model is based on a mean-field approach that is based on MDS data which includes the asymmetry of the induced dipole of the water molecules near the confinement walls. This turns out to be essential in order to explain quantitatively the recent experimental data [20] for $h \geq 15$ Å. It resulted in different quantitative results (as compared to the former C model) for one of the key parameters of the C model (i.e., SL thickness). For channels with thickness $h < 15$ Å, the mean-field approach is no longer applicable and we have to include the microscopic details of water. We obtained small values for ϵ_{\perp} , which are due to the suppression of the fluctuation of the z component of the water dipoles resulting in an order of magnitude decrease of ϵ_{\perp} , as compared to the bulk value (≈ 80). Therefore, there is a significant difference between fluctuations in $m_{\perp}(z)$ for channels with height $h < 15$ Å and that of bulk water. We found that while the diffusion coefficient recovers its bulk value for channels of size $h \geq 15$ Å, there is a long-range effect on the fluctuation of M_z due to confinement. Furthermore, notice that the obtained $\epsilon_{\perp} \cong 2.1$ for height $10 \text{ Å} < h < 15 \text{ Å}$ is much smaller than that of bulk water (≈ 80), proton-disordered ice phases, e.g., ice Ih (≈ 99) [17], low-temperature proton-ordered ices (≈ 3 -4), and many other phases of ice [20]. Although confined water (in channels with height $h < 15$ Å) can be categorized as a random phase of ice, it nevertheless exhibits smaller (larger) dielectric constant (density ρ_z) than all previously known ices. Our modeling and simulations bridge the microscopic theory and continuum mean-field approach (established by Debye, Onsager, and Krikwood [18]) and elucidate the microscopic mechanisms that determine the dielectric properties of confined water.

ACKNOWLEDGMENTS

This work was supported by the Flemish Science Foundation (FWO-VI) and the Methusalem program.

- [1] J. K. Holt, H. G. Park, Y. Wang, M. Stadermann, A. B. Artyukhin, C. P. Grigoropo, A. Noy, and O. Bakajin, *Science* **312**, 1034 (2006).
- [2] D. Takaiwa, I. Hatano, K. Koga, and H. Tanaka, *Proc. Natl. Acad. Sci. USA* **105**, 39 (2008).
- [3] H. Kyakuno, K. Matsuda, H. Yahiro, Y. Inami, T. Fukuoka, Y. Miyata, K. Yanagi, Y. Maniwa, H. Kataura, T. Saito, M. Yumura, and S. Ijima, *J. Chem. Phys.* **134**, 244501 (2011).
- [4] M. Neek-Amal, A. Lohrasebi, M. Mousaei, F. Shayeganfar, B. Radha, and F. M. Peeters, *Appl. Phys. Lett.* **113**, 083101 (2018).
- [5] A. Sugahara, Y. Ando, S. Kajiyama, K. Yazawa, K. Gotoh, M. Otani, M. Okubo, and A. Yamada, *Nat. Commun.* **10**, 850 (2019).
- [6] M. Neek-Amal, F. M. Peeters, Irina V. Grigorieva, and A. K. Geim, *ACS Nano* **10**, 3685 (2016).
- [7] M. Sobrino Fernandez, F. M. Peeters, and M. Neek-Amal, *Phys. Rev. B* **94**, 045436 (2016).
- [8] B. R. H. de Aquino, H. Ghorbanfekr-Kalashami, M. Neek-Amal, and F. M. Peeters, *Phys. Rev. B* **97**, 144111 (2018).
- [9] M. Neumann and O. Steinhauser, *Chem. Phys. Lett.* **95**, 417 (1983).
- [10] M. Neumann, O. Steinhauser, and G. S. Pawley, *Mol. Phys.* **52**, 97 (1984).
- [11] M. Neumann, *J. Chem. Phys.* **82**, 5663 (1985); M. Neumann and O. Steinhauser, *Chem. Phys. Lett.* **102**, 508 (1983).
- [12] H. Sakuma and K. Kawamura, *Geochim. Cosmochim. Acta* **73**, 4100 (2009).
- [13] H. Sakuma, T. Kondo, H. Nakao, K. Shiraki, and K. Kawamura, *J. Phys. Chem. C* **115**, 15959 (2011).
- [14] S. Joseph and N. R. Aluru, *Nano Lett.* **8**, 452 (2008).
- [15] Alexander Schlaich, Ernst W. Knapp, and Roland R. Netz, *Phys. Rev. Lett.* **117**, 048001 (2016).
- [16] V. Ballenegger and J.-P. Hansen, *J. Chem. Phys.* **122**, 114711 (2005).
- [17] J. L. Aragones, L. G. MacDowell, and C. Vega, *J. Phys. Chem. A* **115**, 5745 (2011).

- [18] Daniel C. Elton, Ph.D. thesis, Stony Brook University, 2016.
- [19] S. Varghese, S. K. Kannam, J. Schmidt, H. Sarith, and P. Sathian, *Langmuir* **35**, 8159 (2019).
- [20] L. Fumagalli, A. Esfandiar, R. Fabregas, S. Hu, P. Ares, A. Janardanan, Q. Yang, B. Radha, T. Taniguchi, K. Watanabe, G. Gomila, K. S. Novoselov, and A. K. Geim, *Science* **360**, 1339 (2018).
- [21] Chao Zhang, *J. Chem. Phys.* **148**, 156101 (2018).
- [22] S. Plimpton, *J. Comput. Phys.* **117**, 1 (1995).
- [23] H. J. C. Berendsen, J. R. Grigera, and T. P. Straatsma, *J. Phys. Chem.* **91**, 6269 (1987).
- [24] See Supplemental Material at <http://link.aps.org/supplemental/10.1103/PhysRevE.102.022803> for details about the molecular dynamics simulations method and capacitance model.
- [25] O. Stern, *Z. Electrochem. Angew. Phys. Chem.* **30**, 508 (1924).
- [26] G. Algara-Siller, O. Lehtinen, F. C. Wang, R. R. Nair, U. Kaiser, H. A. Wu, A. K. Geim, and I. V. Grigorieva, *Nature (London)* **519**, 443 (2015).
- [27] G. Cicero, J. C. Grossman, E. Schwegler, F. Gygi, and G. Galli, *J. Am. Chem. Soc.* **130**, 1871 (2008).
- [28] H. G. Kalashami and M. Neek-Amal, and F. M. Peeters, *Phys. Rev. Materials* **2**, 074004 (2018).
- [29] R. Zangi and A. E. Mark, *Phys. Rev. Lett.* **91**, 025502 (2003).
- [30] M. H. Nayfeh and M. K. Brussel, *Electricity and Magnetism* (Courier Dover Publications, Mineola, New York, 2015).
- [31] Hidenosuke Itoh and Hiroshi Sakuma, *J. Chem. Phys.* **142**, 184703 (2015).
- [32] S. Gekle and R. R. Netz, *J. Chem. Phys.* **137**, 104704 (2012).
- [33] V. Satarifard, M. Mousaei, F. Hadadi, J. Dix, M. Sobrino Fernandez, P. Carbone, J. Beheshtian, F. M. Peeters, and M. Neek-Amal, *Phys. Rev. B* **95**, 064105 (2017).
- [34] X. Qin, Q. Yuan, Y. Zhao, S. Xie, and Z. Liu, *Nano Lett.* **11**, 2173 (2011).
- [35] Yanbin Wu, L. K. Wagner, and N. R. Aluru, *J. Chem. Phys.* **144**, 204903 (2016).
- [36] S. Ghasemi, M. Alihosseini, F. Peymanirad, H. Jalali, S. A. Ketabi, F. Khoeini, and M. Neek-Amal, *Phys. Rev. B* **101**, 184202 (2020).